Tuning the Electronic Properties of Rotated Graphene on Ni(111) by Nickel Carbide Intercalation

Jiaming Song, Matthias Bernien, Chii-Bin Wu[1], Wolfgang Kuch*

Freie Universität Berlin, Institut für Experimentalphysik, Arnimallee 14, 14195 Berlin, Germany

* kuch@physik.fu-berlin.de; Tel.: +49-30-838-52098; Fax.: +49-30-838-452098

[1] Present affiliation: Chung Yuan Christian University, Department of Physics, Chungli 32023 Taiwan, R. O. C.

Abstract

High-temperature-deposited rotated graphene (Gr) on Ni(111) has been investigated by *in-situ* scanning tunneling microscopy and spectroscopy at room temperature. The rotated Gr exhibits weak bonding to the Ni(111) surface, which facilitates formation of Ni_2C or a second Gr layer underneath via bulk carbon segregation. Areas of rotated Gr present a bias voltage dependence of the apparent amplitude of Gr superlattice corrugations. We find that Ni_2C underneath rotated Gr introduces additional electronic features that vary with the gap resistance, which could be related to an orientation-dependent interaction between Ni_2C and Gr. Furthermore, the exposure to oxygen has a significant influence on the local density of states of Gr/Ni_2C, other than on Ni(111) covered with nonrotated Gr.

1. Introduction

Low-dimensional materials exhibit unique properties influenced by quantum size effects. One prominent example is the 2D carbon crystal with honey-comb lattice, graphene (Gr).[1] In the past decade, Gr has attracted great attention because of its extraordinary properties such as high mechanical strength,[2] excellent heat and electrical conductance,[3] and very high transmittance.[4] Gr has extremely small spin-orbit interaction and almost zero nuclear magnetic moment, facilitating room-temperature spin current injection and detection, and therefore, it is an excellent candidate for spin qubits in quantum computing.[5] Gr-based spintronics has a great potential in spintronic device applications and is becoming more and more attractive.[6,7] Spin filtering at the interface between graphite and close-packed fcc Ni(111) or hcp Co(0001) has been predicted by Karpan et al.[7,8] The spin-valve effect for a ferromagnetic (FM) transition metal in contact with Gr has also been reported.[9–11] Moreover, besides the 2D sheet, Gr can be wrapped up into 0D buckyballs, rolled into 2D nanotubes, or stacked into 3D graphite.[12] Each different form outstretches diverse properties and thus applications.

There are several ways for the preparation of Gr. Besides the exfoliation technique, chemical vapor deposition (CVD) is an important method, in which a substrate is necessary. When Gr is epitaxially grown on a crystalline substrate, there is a registry between the two. Depending on the substrate, the properties of Gr are modified compared to ideal free-standing Gr. For transition metal substrates, a strong hybridization between the Gr π band and the metal *d* bands can introduce charge transfer from the substrate and modify the electronic properties of Gr greatly.[13–15] Under this circumstance, the Fermi energy may not be necessarily at the Dirac point and can be

tuned by intercalation of other atoms[16–18] or small molecules.[19,20] Moreover, different adsorption geometries for Gr on the metal substrate can coexist.[21,22] Nickel, due to its catalytic property in CVD, has been utilized as substrate for the growth of Gr in recent years. Because of the almost perfect match of Ni(111) and graphite lattice parameters, Gr/Ni(111) is attracting more and more attention.[23] Although compared to other substrates,[24–29] Ni(111) matches Gr best, the preparation conditions, such as temperature,[30,31] carbon concentration at the growth front,[31] purity of the substrate,[31] or cooling rate,[32,33] can influence the quality of the Gr sheets on the nickel substrate, such that the structure formed on the sample surface could be far more complicated than expected.[31] Besides the (1×1)-restricted Gr, rotations, extra carbon structures underneath, or surface defects may also exist and influence the Gr interaction with the substrate. These unexpected structures exhibit unique structural and electronic properties which may be interesting for Gr-based electronic and spintronic applications.

To understand the growth mechanism of Gr on bulk Ni(111) at high temperatures ($\geq$ 900 K), high-resolution scanning tunneling microscopy (STM) provides a direct way of *in-situ* characterization of the ultrahigh-vacuum-grown Gr in real space and facilitates understanding of Gr electronic properties near the Fermi energy. STM studies of Gr deposition on Ni(111) have been reported by several researchers. One debating theme among these studies is the formation of nickel carbide (Ni_2C). Lahiri et al. suggest that Gr grows via an in-plane transformation of Ni_2C.[34] By fast-Fourier-transform (FFT) analysis, Jacobson et al. proposed that areas similar to those observed in Ref. [34] should be Gr-covered Ni_2C rather than exposed Ni_2C as identified in Ref [34].[35] Jacobson et al. found that Ni_2C only exists underneath rotated-Gr areas and suggest

the earlier formed Ni_2C causes the grain rotation of the later-on-formed Gr.[35] Very soon afterwards, an *in-situ* STM observation of Gr growth on Ni(111) reported by Patera et al. proposed an opposite mechanism, namely that in Gr/Ni_2C areas, the formation of Ni_2C via bulk carbon segregation happens after the formation of rotated Gr on Ni(111).[31] It means that the later-on-formed Ni_2C does not influence the grain orientation of the topmost Gr layer. Nevertheless, in both, Refs. [35] and [31], Gr/Ni_2C areas only exist when the top Gr exhibits some degrees of rotation with respect to the Ni(111) substrate. No further carbon structure could be found underneath (1×1) epitaxial Gr. On Ni(111), (1×1) epitaxial Gr can be tightly chemisorbed to the metal substrate, while some degrees of rotation can weaken the bonding between Gr and the substrate. Rotated Gr exhibits diverse structural and electronic properties when grown on a bulk Ni(111) single crystal, which is the main focus of this paper. Here, we present a detailed STM investigation into Gr on Ni(111) grown by CVD at high temperature. We find that Gr/Ni_2C can be present also rotated by different angles than those reported before. We observe that the apparent corrugation of rotated Gr depends not only on the rotation angle, but also on the bias voltage. The electronic properties of Gr-covered Ni_2C are furthermore influenced by the tunneling gap and the Gr orientation. Finally we address the oxygen-induced tuning of the electronic properties of rotated graphene on Ni_2C.

2. Experimental details

The experiment was performed in an ultrahigh vacuum (UHV) chamber with a base pressure of 1×10^{-10} mbar. A disk-shaped Ni(111) single crystal with a diameter of 10 mm was used as substrate. To achieve well-defined surfaces, the Ni(111) substrate was cleaned by cycles of Ar^+

sputtering with ion energy of 1 keV at 700~750 K, followed by subsequent annealing at 950 K for 20~30 minutes. The cleanliness and smoothness of the crystal surface was examined by Auger electron spectroscopy (AES), low-energy electron diffraction (LEED), and STM. The Gr growth was performed in UHV by CVD, employing propylene with 99.95% purity as the carbon source. We studied two different preparation recipes:[36]

Recipe (1): Dosing propylene at 900 K, 1×10^{-5} mbar for 5 min [3000 L (Langmuir, 1 L=10^{-6} mbar·s)], followed by 20 min annealing at 920 K;

Recipe (2): Dosing propylene at 900 K, 2.5×10^{-6} mbar for 10–20 min (1500–3000 L), no subsequent annealing.

In both recipes, the sample is cooled naturally in UHV [roughly 60 min from 920 K to 300 K]. A room-temperature STM (Omicron 1) was used for the STM measurements. A lock-in amplifier (modulation voltage and frequency: 20 mV, 2.38 kHz) facilitates extracting the *dI/dV* signal and scanning tunneling spectroscopy (STS) is obtained simultaneously with the constant-current topography during the scanning process.

3. Results and discussion

3.1 Structures formed on the Ni(111) surface

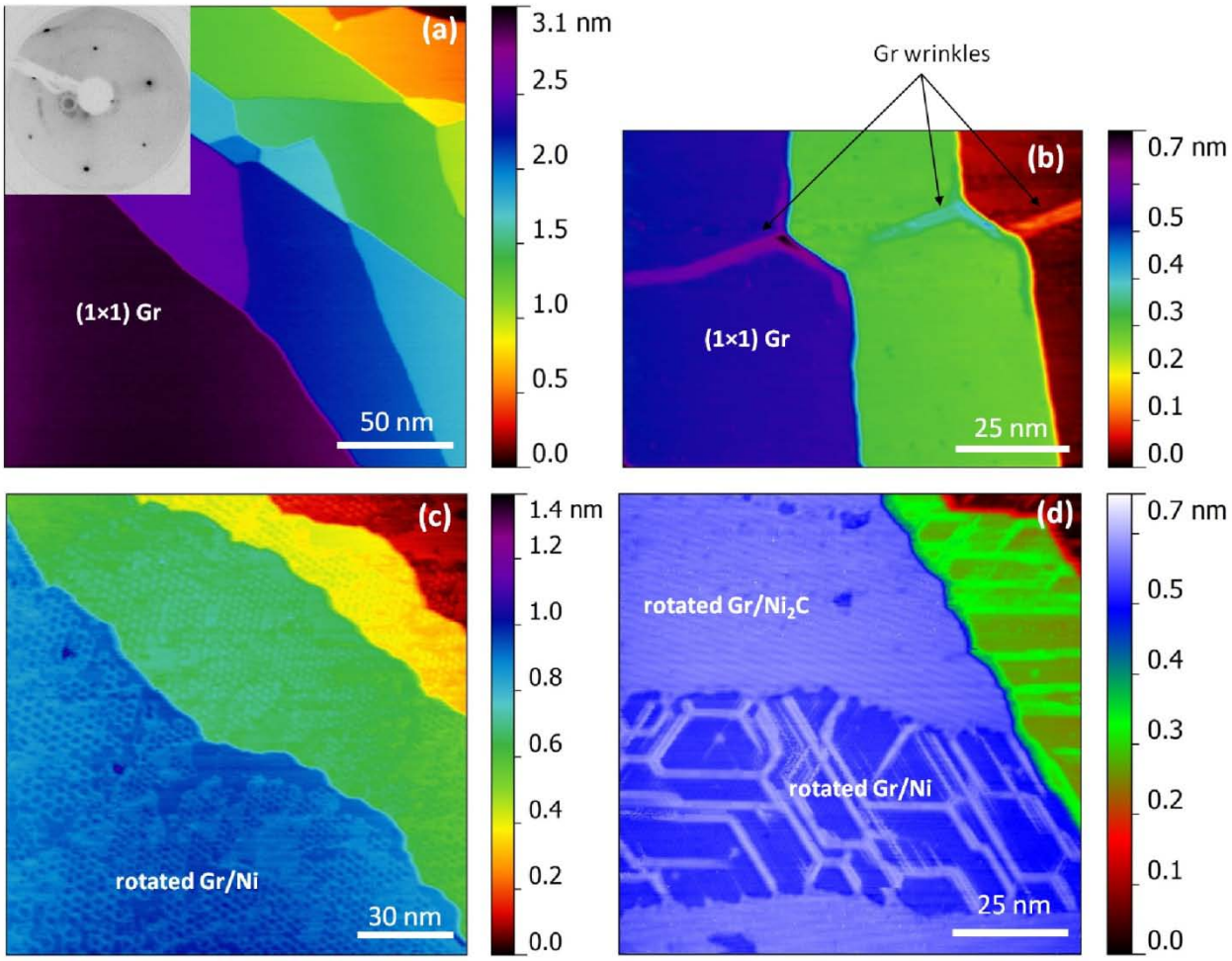

Figure 1 Constant-current STM images for the sample prepared by recipe (1). (a), (b) Mostly observed (1×1) Gr on the sample surface. The inset of (a) is a LEED pattern obtained from the same sample at 149 eV. (c), (d) Occasionally observed rotated Gr. Feedback parameters: (a) +1.00 V, 2.40 nA; (b) +0.81 V, 2.13 nA; (c) +1.00 V, 2.61 nA; (d) +0.99 V, 2.35 nA.

We will first give a short overview of the structures formed on the Ni(111) surface after growth according to the two recipes. Figure 1 shows STM topography images of Gr prepared by recipe (1). A similar morphology as shown in Figure 1a and b is also observed in most of the other areas

on the sample surface. These areas only exhibit smooth and flat (1×1) Gr on Ni(111), consistent with the LEED pattern shown in the inset of Figure 1a. However, there are still some small exceptional areas that exhibit a different morphology, as shown in Figure 1c and d. In panel c, rotated Gr on Ni(111) is observed, as the hexagonal superlattice on part of the terraces illustrates. In contrast, panel d shows Gr on different structures underneath. There are mainly two types of structures underneath the Gr layer, i.e., Ni(111) and Ni_2C. Similar topographies have also been observed before, i.e., the Gr/Ni_2C area exhibits stripe features and the Gr/Ni(111) area exhibits superlattices.[31,35] The carbon concentration is an important factor for the Gr growth at high temperatures. If the concentration is not high enough to form another Gr layer, carbides will grow instead,[23,31,37] as shown in Figure 1d.

The LEED pattern of Gr prepared by recipe (2) does not differ from that shown in Figure 1a, indicating a dominating (1×1) Gr surface. However, on this sample surface, some unique areas have been observed, as shown in Figure 2. Compared with the ML Gr on Ni_2C, the STM images in Figure 2 show not only a ML Gr on Ni_2C/Ni(111), but also BL Gr on Ni(111). This is seen from the areas marked with "B". Here the 2D FFT in Figure 2e demonstrates two sets of hexagonal patterns, as the red and blue circles illustrate. The inset of Figure 2d is the 2D-FFT filtered [using the two sets of hexagonal superlattices marked by red and blue circles in Figure 2e] image for area "B". There are two superlattices with six-fold symmetry and different periodicities, as the blue and red hexagons show. The blue and red hexagons correspond to two sets of patterns marked by the same colors in Figure 2e. The real-space periodicities are 0.75 nm and 3.55 nm, respectively. These two superlattices are due to the non-Bernal stacking[38,39] of two

Gr layers with rotation angles of 18.9° and 4°, respectively, with respect to the [1-10] direction of the Ni(111) substrate. The calculated angles are consistent with the rotation angles for the two sets of patterns in Figure 2e, that indicate a misorientation angle of 22.9° between the two Gr sheets.

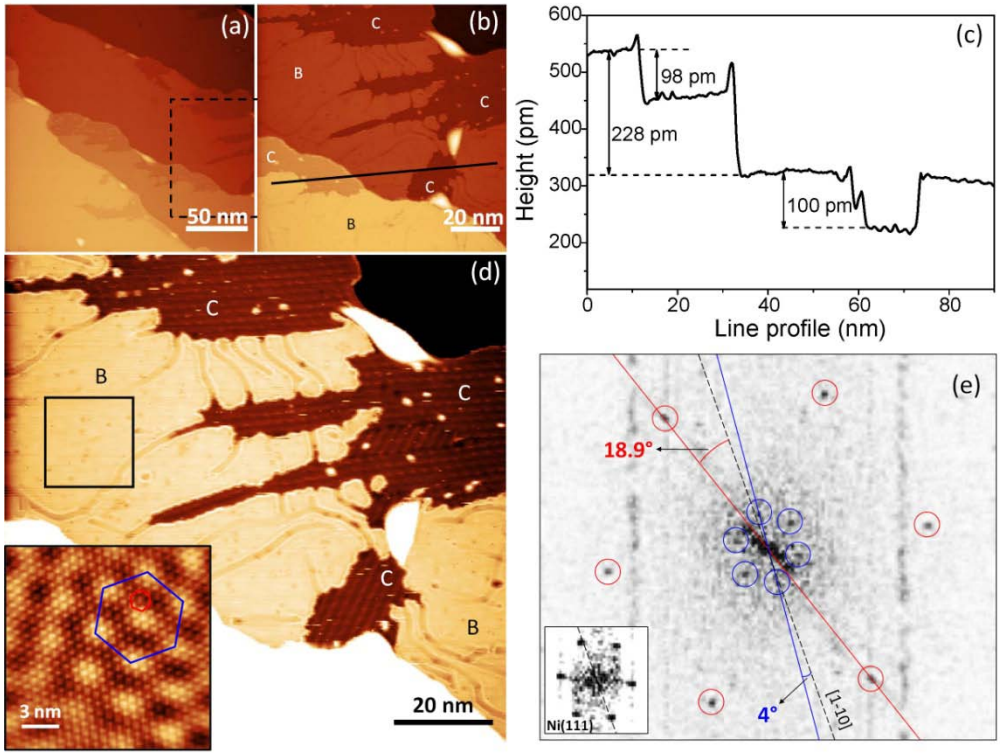

Figure 2 (a), (b), (d) Constant-current STM images of a sample prepared by recipe (2). Feedback parameters: +1.1 V, 0.49 nA. Part of (b) shows the zoomed-in image of the area marked by the dashed rectangle in (a). (c) Line profile along the black line in (b). (d) illustrates the same area as (b) but with enhanced image contrast on one terrace. Areas marked with "B" and "C" represent BL Gr/Ni(111) and ML Gr/Ni_2C/Ni(111), respectively. The inset is the 2D FFT-filtered [filtered by the selected hexagonal spots marked by red and blue circles in (e)] area for the BL Gr/Ni(111) marked by the black square in (d). The red and blue hexagons correspond to two sets of patterns marked by the same colors in (e). (e) 2D FFT of area "B" in (d). The inset of (e) is the 2D FFT of the clean Ni(111) surface imaged with atomic resolution. The dashed black line demonstrates the [1-10] direction of the Ni(111) substrate. Red and blue circles mark the two superlattices caused by the misorientation of the two non-Bernal-stacked Gr layers.

The main difference between preparation according to recipes (1) and (2) is the formation of BL Gr in the latter. The presence of a minority amount of rotated Gr, both on Ni(111) as well as on Ni_2C/Ni(111), is confirmed for both preparation recipes.

3.2 Dependence of apparent corrugation of rotated Gr on orientation angle and bias voltage

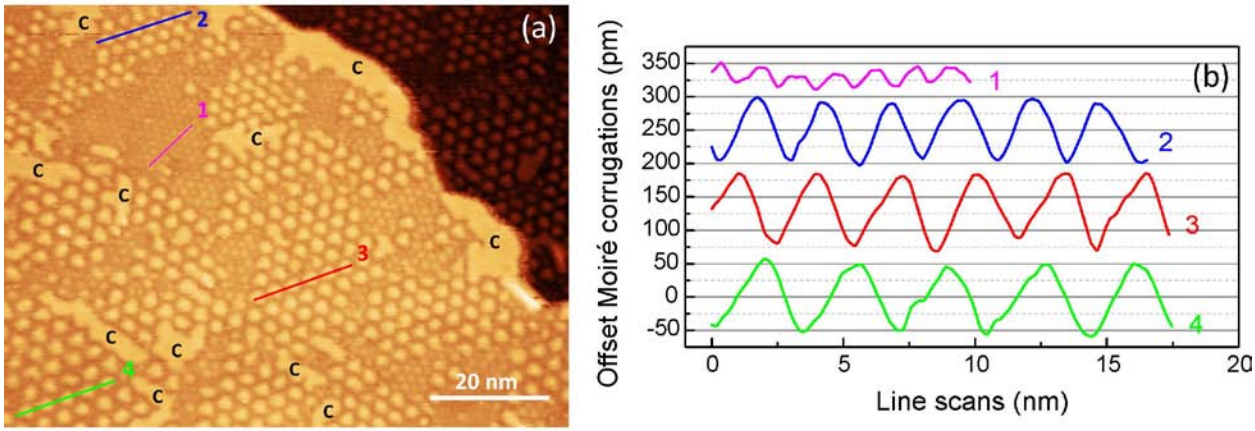

Figure 3 (a) Constant-current STM image of a ML of rotated Gr/Ni(111) (+0.2 V, 2.6 nA). Areas marked by "C" illustrate Gr on Ni_2C. (b) Line scans along lines marked with the same numbers in (a).

In the following, since rotated Gr exhibits diverse structures, we will discuss the structure-related electronic properties of rotated Gr. The rotated Gr monolayer (ML) has a relatively weak bonding to the supporting Ni(111) surface compared to epitaxial Gr/Ni(111).[40,41] A Gr-covered surface with superlattices of different periodicities, prepared by recipe (1), is shown in Figure 3a. The origin of the observed superlattices has been discussed by several researchers[42–47] and the most widely accepted explanation is the Moiré assumption.[48,49] The Moiré pattern originates from the

misalignment of two periodic layers,[50,51] which, by electronic interference, leads to a superstructure of the local density of states (LDOS) on the surface and thus of the tunneling current. In Gr on the Ni(111) surface, Moiré patterns have been already observed by several researchers[23,31,33–35,38,52]. The relation between the Moiré superlattice periodicity *D*, the atomic spacing *d* of graphite, and the Gr misorientation angle θ is expressed by $D = d/[2\ \sin(\theta/2)]$.[48] In Figure 3a, there are mainly four types of Moiré patterns. Line scans 1, 2, 3, 4 illustrate periodicities of 1.45 nm, 2.6 nm, 3.04 nm, 3.54 nm, which correspond to rotation angles of 9.8°, 5.4°, 4.6°, 4°, respectively. Between two adjacent grains of dissimilar Moiré periodicities, no distinct boundaries can be found, which differs from the STM observation of beads-like boundaries[53–60] between AB-stacked Moiré regions and AA-stacked non-Moiré regions on graphite. The beads-like boundary is due to chiral edge states of twisted bilayer (BL) graphite sheets in AB-stacked regions,[60] which hence should not be the present here in Figure 3a. Once Gr starts to nucleate on Ni(111), the subsequent growth will follow the initial stacking sequence. In the STM image, the multiperiodic Moiré patterns are probably due to different rotation angles for different Gr nucleation centers at the very beginning of the growth, such that after small fragments of Gr get bonded to each other and form a whole sheet, the as-grown patterns are formed. Accordingly, due to the misorientation of the adjacent Gr patches, at the boundary positions, defects or dislocations are likely to exist.[61–63]

The amplitudes of the observed Moiré patterns show significant differences depending on their periodicity. Smaller periodicity, as profile 1 shows, corresponds to larger rotation angle and demonstrates a much smaller amplitude of 40 pm compared to that of 114 pm for profile 4. This

rotation-angle-dependent Moiré pattern corrugation indicates a periodic electronic-interaction tuning by modulating the Gr orientation with respect to the supporting substrate and might be of interest for applications in molecule or cluster self-assembly.

The areas marked by "C" are similar to those reported in Ref. [34], which have been interpreted as pure Ni_2C that could be further converted into Gr. However, this interpretation proves to be a misidentification of Gr/Ni_2C in the supplementary material of Ref. [35]. The morphology of Gr/Ni_2C does not exhibit any Moiré pattern with hexagonal symmetry. It is formed from a honeycomb lattice on a quasi-square lattice.[35] Accordingly, here the areas marked with "C" are supposed to be Gr-covered Ni_2C, which originates from bulk carbon segregation.

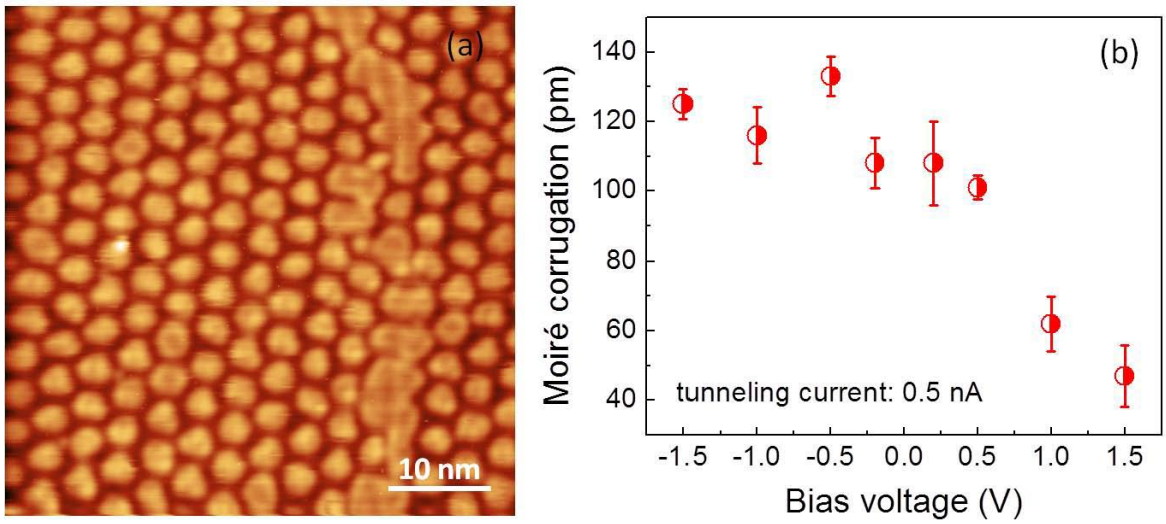

Figure 4 (a) Constant-current STM image for a ML Gr/Ni(111) (+1.0 V, 0.5 nA). (b) Moiré corrugation of the rotated Gr shown in (a) at different bias voltages.

The Moiré corrugation does not only vary with the Gr rotation angle as discussed above, it can also be tuned by the bias voltage applied between tip and sample. Figure 4a shows an STM topography image of a ML of rotated Gr/Ni(111) with a Moiré periodicity of about 3.53 nm, prepared by recipe (1). By varying the bias voltage from –1.5 V to +1.5 V, the amplitude of the apparent Moiré corrugation decreases from 125 pm to 48 pm. A similar phenomenon has been reported in Gr/Ru(0001).[64,65] The electronic effect plays an important role for compensating the surface Moiré corrugation by 0.16 nm[66,67] for Gr/Ru(0001). Atomically-resolved STM imaging and DFT calculations for the same system revealed that STM images at low bias voltages mainly reflect the geometrical corrugation while at higher voltages, an electronic resonance state has significant influence on the periodic distribution of the LDOS and local work function of Gr.[68] An angle-resolved photoemission spectroscopy (ARPES) study on epitaxial Gr on Ni(111) revealed that the Dirac cone is shifted downward by 2.84 eV to higher binding energy with respect to a freestanding Gr sheet because of hybridization of the Gr π orbital with nickel 3*d* states.[69] Although shifted, the Dirac cone remains intact and no gap opening is found at the Dirac energy.[69] A down shift of the Dirac cone of about 2.0 eV compared to a quasi-freestanding Gr layer was also discovered elsewhere.[17] This shift indicates a strong *n*-type doping of Gr by dynamical hybridization of Gr on the Ni(111) surface,[69] which influences the charge transfer from nickel to Gr. As to the rotated Gr on Ni(111), a hybridization of the Gr π band and the nickel 3*d* band could also occur and thus modify the electronic properties of Gr.[40] The dynamic hybridization between nickel 3*d* and Gr exhibits an energy dependence which might lead to different doping levels of Gr at different energies[69] and has an impact on the charge transfer from metal to Gr.[70] Accordingly, in Figure 4b, the observed reduction of the Moiré corrugation at

higher bias voltages could be due to an electronic effect which might be caused by the varying charge transfer from the metal substrate.

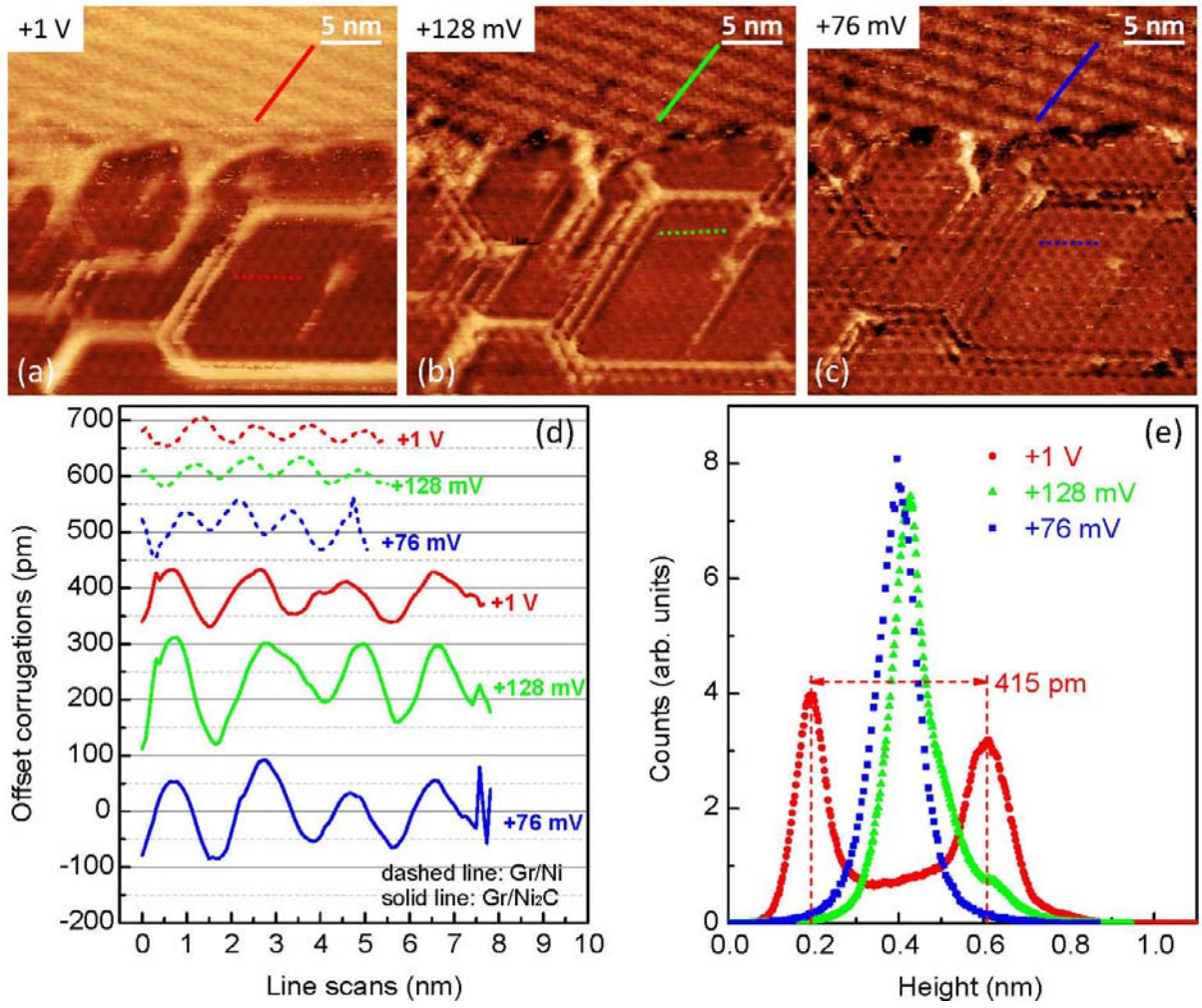

Figure 5 (a), (b), (c) Constant-current STM images for rotated ML Gr at +1V, +128 mV, +76 mV, respectively. Feedback current: 2.35 nA. This area is from a smaller part of the area shown in Figure 1d. (d) Line scans along lines in (a), (b), (c). (e) Histograms for (a), (b), (c).

STM does not only image the structures on the surface, but also screens the underlying structures that also contribute to the surface electron distribution.[49] When Ni_2C is formed between rotated Gr and the Ni(111) surface, the Gr Moiré pattern disappears. The upper part of the STM images in Figure 5 shows Gr-covered Ni_2C, while the lower part consists of rotated Gr/Ni(111) with a Moiré periodicity of about 1.22 nm. The sample was prepared according to recipe (1). At different bias voltages, the two areas demonstrate distinct corrugation behaviors and in general, the Gr in contact with Ni_2C exhibits a larger corrugation with a periodicity of 1.95 nm, which is close to the value reported for Gr/Ni_2C.[35] For a low bias voltage of +76 mV, both upper and lower areas show high corrugations of 175 pm and 90 pm, respectively, while at +1 V, the corrugation is reduced by 78 pm and 37 pm, see Figure 5d. Moreover, at +128 mV Gr/Ni(111) turns out to have a similar corrugation as at +1 V, but Gr/Ni_2C still maintains a similar amplitude compared to the lower bias voltage of +76 mV. Histograms for the two different regions in Figure 5e show that there is an apparent step height of about 415 pm between Gr/Ni(111) and Gr/Ni_2C at the bias voltage of +1 V, while this step vanishes close to the Fermi energy. This phenomenon clearly shows that there is an electronic charge inhomogeneity between the two regions. In the areas with Ni_2C underneath Gr, nickel *d* orbitals bind to carbon 2*p* orbitals, which could drastically modify the electronic environment of the Gr sheet and the corresponding doping. Compared to the quasi-freestanding topmost layer of a bilayer (BL) Gr or graphite, Gr/Ni_2C might also possess some degree of “free-standing” property with less influence of the 3*d* metal, and the interacting force between Gr and Ni_2C might not necessarily be as weak as van der Waals interaction between Gr layers. Compared to the decoupling of Gr via intercalation of metal[16–18,71–

[86] or nonmetal[19,20,87–90] clusters, the Ni_2C-introduced decoupling of Gr from the contacting surface might be another topic of interest for future studies.

3.3 Influence of the tunneling gap and the Gr orientation on the electronic properties of Gr-covered Ni_2C

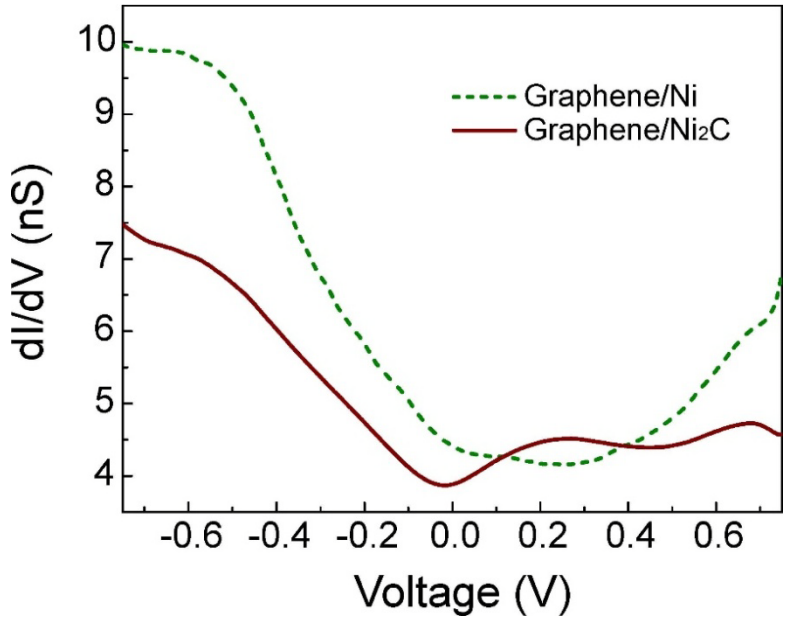

Figure 6 STS curves of Gr/Ni(111) (dashed line) and Gr/Ni_2C/Ni(111) (solid line) taken from the respective areas in Figure 5. Feedback parameters: +0.5 V, 2.35 nA.

When Ni_2C is formed between the nickel surface and the rotated Gr layer, the LDOS of Gr is completely changed, as the STS curves in Figure 6 show. Below the Fermi energy, the occupied LDOS is reduced compared to that without Ni_2C. At a bias voltage of about +0.2 V, the STS curve of Gr/Ni_2C exhibits a small peak. Around this energy the density of unoccupied states is slightly higher than that in Gr/Ni(111). Since the carbon 2*p* orbitals in Ni_2C bind to the nickel 3*d*

orbitals, the hybridization between nickel 3*d* and Gr π orbitals might be weakened, which could be one possible reason for the higher density of unoccupied states at energies near 0.2 eV and the lower density of occupied states of Gr/Ni_2C.

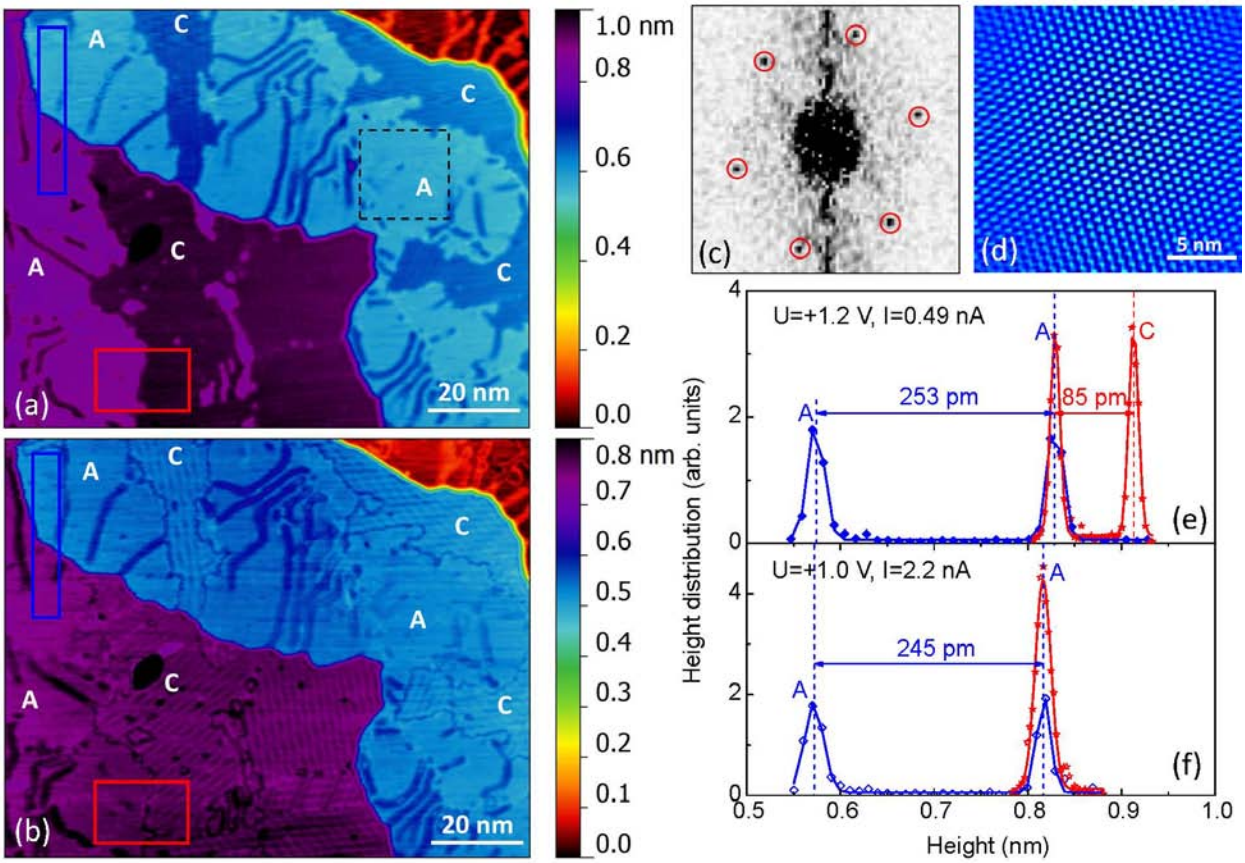

Figure 7 (a), (b) Constant-current STM images of a rotated Gr ML. Feedback parameters: (a) +1.2 V, 0.49 nA; (b) +1.0 V, 2.2 nA. Areas marked with “A” and “C” represent Gr/Ni(111) and Gr/Ni_2C/Ni(111), respectively. (c) 2D FFT of part of area A as marked by the dashed square in (a) and the corresponding 2D-FFT-filtered [filtered by the selected hexagonal spots marked by red circles in (c)] image (d). (e), (f) histograms for areas marked with blue and red rectangles in (a) and (b).

The electronic environment of rotated Gr in direct contact with Ni(111) differs from that in contact with Ni_2C, as the discussion about the bias-dependence in section 3.2 illustrates. In the

STM experiment, the tunneling gap also plays an important role in tuning the electronic properties of the surface. The STM images in Figure 7a and b are from almost the same area of a sample prepared according to recipe (1) at similar bias voltages, but the tunneling gap resistance is different [2449 MΩ for a and 455 MΩ for b]. Three terraces are exposed and on each terrace there are two different areas which are identified as Gr/Ni(111) (areas marked with "A") and Gr/Ni_2C (areas marked with "C"). The 2D FFT of area A is shown in Figure 7c and the corresponding filtered image exhibits a Moiré superlattice with a period of about 0.72 nm, which corresponds to a rotation angle of 19.7° of the Gr sheet. Histograms shown in Figure 7e and f illustrate that when there is a larger tunneling-gap resistance (2449 MΩ), area C appears to be 85 pm higher than area A, while the apparent height difference vanishes when the tunneling-gap resistance is reduced to 455 MΩ. On the other hand, the tunneling-gap resistance has a much smaller influence on the apparent height difference between adjacent terraces with only Gr/Ni(111), which is close to the interlayer distance of the fcc Ni(111) single crystal. The disappearance of the height difference between areas A and C caused by the change in tunneling-gap resistance further indicates that the interaction between Gr and Ni_2C can be drastically tuned electrically by the tunneling electrodes. With a smaller gap resistance, the tunneling electrons mainly reflect the geometrical structure of the surface and Gr/Ni(111) and Gr/Ni_2C/Ni(111) have the same height, while with a larger gap resistance the electronic structure is dominating, leading to a higher conductivity of the Gr/Ni_2C/Ni(111) region. When comparing Figure 7b and Figure 5a, in contrast, where the tunneling-gap resistance is similar, in Figure 5a, a large height difference of 415 pm is measured between areas of Gr/Ni(111) and of Gr/Ni_2C, while in Figure 7b there is no height difference. This can be explained when considering the different rotation angle of the

two Gr sheets. As already mentioned, the Moiré periodicity for Gr/Ni(111) in Figure 5a is 1.22 nm, which corresponds to a rotation angle of 11.6°, while the rotation angle in Figure 7b is 19.7°. After the formation of a rotated single Gr layer, the subsequently formed Ni_2C underneath[31] should not change the original orientation of the Gr. Therefore, with similar gap resistance, the reason for the difference between Figure 5a and Figure 7b has to be the different orientation angle of Gr with respect to the Ni(111) substrate.

3.4 Tuning the electronic properties of rotated Gr on Ni_2C by oxygen

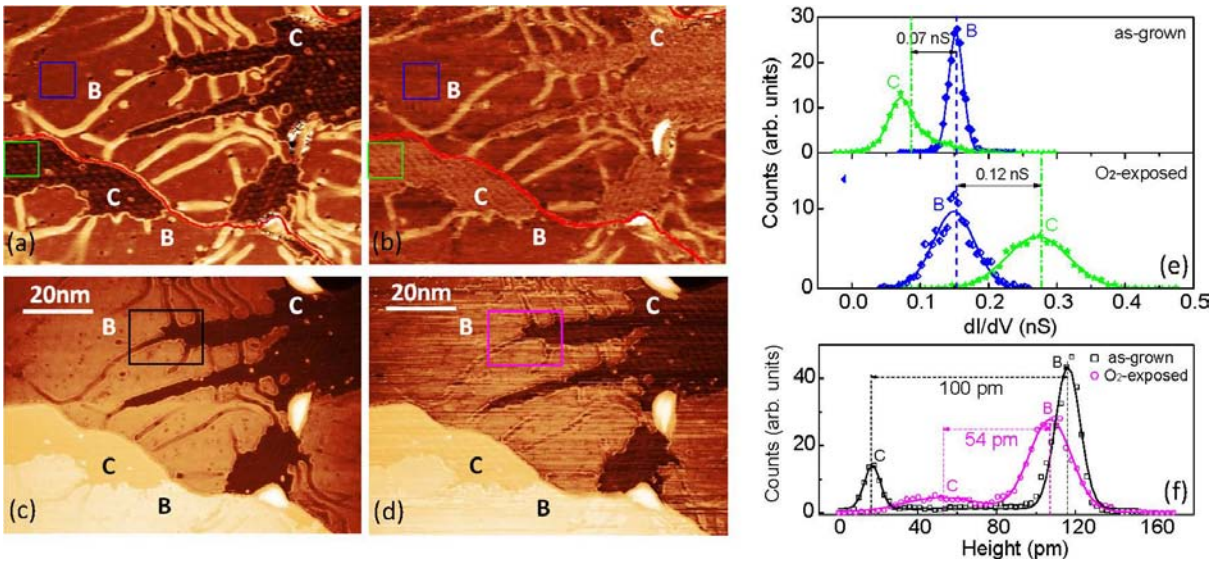

Figure 8 (a), (b) Constant-current STM differential conductance maps for pristine Gr and Gr exposed to 1050 L oxygen, respectively. (c), (d) Simultaneously recorded topographies for (a), (b). The scanning area is from the same position as shown in Figure 2d. Feedback parameters: +1.0 V, 0.5 nA. Areas marked with "B" and "C" represent BL Gr/Ni(111) and ML Gr/Ni_2C/Ni(111), respectively, consistent with Figure 2d. (e) Top and bottom are histograms for the areas marked by blue and green squares in (a) and (b). (f) Histograms for areas marked with black and pink rectangles in (c) and (d). Red lines in (a) and (b) illustrate terrace borders. Vertical dashed lines in (e) represent averaged values and in (f) maximum values for the respective areas.

It has already been shown that a Gr-covered Ni(111) surface is protected from oxidation.[91,92] If Ni_2C is formed underneath rotated Gr, will the top Gr still be able to protect the material underneath from oxygen? The STM images shown in Figure 8 are from a similar area as those shown in Figure 2b and display the coexistence of BL Gr/Ni(111) ("B") and ML Gr/Ni_2C ("C"). In the bottom panel of Figure 8, (c) and (d) are topographies of the same area before and after

exposure to 1050 L oxygen at room temperature, respectively. In the top panel, (a) and (b) are the corresponding simultaneously recorded differential conductance maps. To analyze quantitatively, histograms in Figure 8e show the differential conductances before and after oxygen exposure for area “B” [BL Gr/Ni(111)] and area “C” [ML Gr/Ni_2C/Ni(111)]. The differential conductance in area “B” is 0.07 nS higher than that in area “C” for the as-grown surface, while the contrast reverses after oxygen exposure when the differential conductance for Gr-covered Ni_2C is 0.19 nS higher than before. The BL Gr/Ni(111) remains unaffected by the oxygen dosage, which is consistent to a previous study on the Gr passivation of the Ni(111) surface.[91] The unchanged differential conductance in areas “B” implies similar tip conditions before and after oxygen exposure. Moreover, histograms for the corresponding topographies also demonstrate a relative height reduction of 46 pm between areas “B” and “C” by the oxygen influence, as seen in Figure 8f. A slight shift of 10 pm between the two peaks marked with “B” in Figure 8f is due to the piezo drift between two separate scanning processes.

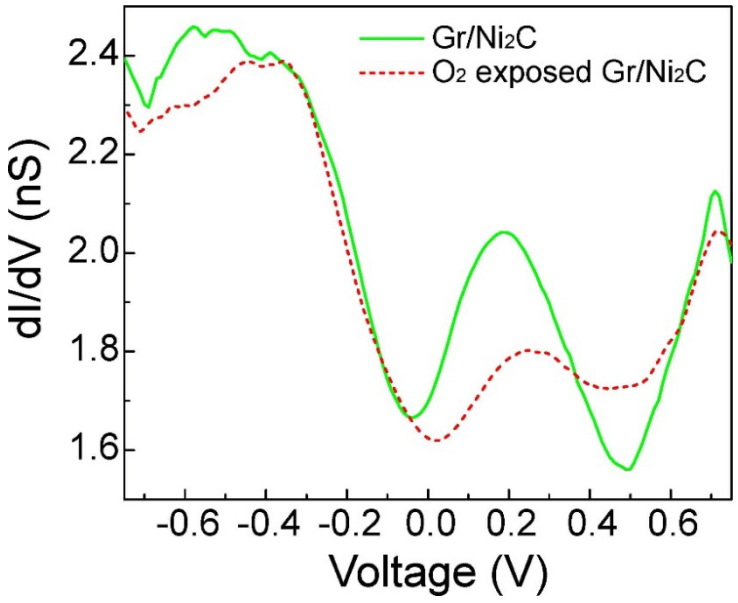

Figure 9 STS of pristine (solid line) and 160 L oxygen exposed (dashed line) Gr/Ni_2C/Ni(111). Feedback parameters: +0.5 V, 1.8 nA.

The STS curves for Gr/Ni_2C (areas "C") shown in Figure 9 indeed illustrate a distinguished electronic modification after a small amount of oxygen dosage. In the spectra here, a similar peak at +0.2 V as the one shown before in Figure 6 is reduced after dosing oxygen, indicating a decrease in the density of unoccupied states at that energy, whereas the valley at +0.5 V is higher than before. Considering also the less deep contrast level of the Gr/Ni_2C regions in Figure 8b (bias voltage: +1.0 V), it seems that above the Fermi energy, there is a *dI/dV* contrast oscillation with energy before and after oxygen exposure, as seen in Figure 9. The STS curves also illustrate that oxygen mainly influences the unoccupied states but has little influence on the occupied states near the Fermi level. This electronic modification of Gr/Ni_2C by oxygen suggests that due to the existence of Ni_2C between Gr and the nickel substrate, the Gr passivation effect fails. One

possible scenario could be the intercalation of oxygen between Gr and Ni_2C. Subsequent oxidation of Ni_2C under the Gr layer could then change the electronic environment underneath the Gr layer. According to previous studies[20,87,88,90,93,94] on oxygen intercalation between Gr and the metal surface, the intercalation normally occurs at temperatures higher than room temperature. Therefore, it seems that this scenario is not very likely here. But since the interaction between Gr and the Ni_2C underneath is weak and driven only by van der Waals interaction,[35] this possibility cannot be ruled out. Another scenario could be that due to the formation of Ni_2C, some electronic defects are introduced in the topmost Gr layer, which locally modify the desorption energy barrier of the Gr surface and trap oxygen at these defect sites.[92,95] Since Ni_2C exhibits a periodic structure,[31,35] if such Ni_2C-introduced defects in the topmost Gr layer exist, the Gr layer will exhibit some periodic defects. These defects could act like a quantum dot array, which would be interesting for the application in Gr-based electronic devices.

4. Conclusion

Gr grown at 900 K on Ni(111) has been investigated by STM and STS. Mainly (1×1) epitaxial nonrotated Gr has been observed on the sample surface, but also a small fraction of rotated Gr is present. Due to the weakened bonding between rotated Gr and the Ni(111) surface, further carbon-related structures are formed in between via bulk carbon segregation, namely Ni_2C or a second layer of Gr. The Gr on Ni_2C exhibits quite different electronic properties compared to Gr/Ni(111) and the segregated carbon atoms which form the Ni_2C drastically modify the electronic environment of the Gr layer. The bias dependence of Moiré corrugations of Gr on both Ni_2C and Ni(111) indicates a tuning of the doping level in Gr by the material contacting the Gr

from below. Gr/Ni_2C exhibits rotation-angle-dependent electronic properties, reflecting an orientation-dependent interaction between Gr and Ni_2C. Moreover, Gr on Ni_2C proves not to protect the Ni_2C underlayer from oxidation, which is probably due to Ni_2C-introduced surface defects (either structurally or electronically). Such defects could act as quantum traps for adsorbed oxygen.

Acknowledgments

J. Song acknowledges financial support by the China Scholarship Council (Grant No. 2011628009).

References

(1) Novoselov, K. S.; Geim, A. K.; Morozov, S. V.; Jiang, D.; Zhang, Y.; Dubonos, S. V.; Grigorieva, I. V.; Firsov, A. A. Electric Field Effect in Atomically Thin Carbon Films. *Science* **2004**, *306*, 666–669.

(2) Lee, C.; Wei, X.; Kysar, J. W.; Hone, J. Measurement of the Elastic Properties and Intrinsic Strength of Monolayer Graphene. *Science* **2008**, *321*, 385–388.

(3) Chen, J.-H.; Jang, C.; Xiao, S.; Ishigami, M.; Fuhrer, M. S. Intrinsic and Extrinsic Performance Limits of Graphene Devices on SiO2. *Nat. Nanotechnol.* **2008**, *3*, 206–209.

(4) Bonaccorso, F.; Sun, Z.; Hasan, T.; Ferrari, A. C. Graphene Photonics and Optoelectronics. *Nat. Photonics* **2010**, *4*, 611–622.

(5) Trauzettel, B.; Bulaev, D. V.; Loss, D.; Burkard, G. Spin Qubits in Graphene Quantum Dots. *Nat. Phys.* **2007**, *3*, 192–196.

(6) Tombros, N.; Jozsa, C.; Popinciuc, M.; Jonkman, H. T.; van Wees, B. J. Electronic Spin Transport and Spin Precession in Single Graphene Layers at Room Temperature. *Nature* **2007**, *448*, 571–574.

(7) Karpan, V. M.; Giovannetti, G.; Khomyakov, P. A.; Talanana, M.; Starikov, A. A.; Zwierzycki, M.; van den Brink, J.; Brocks, G.; Kelly, P. J. Graphite and Graphene as Perfect Spin Filters. *Phys. Rev. Lett.* **2007**, *99*, 176602.

(8) Karpan, V. M.; Khomyakov, P. A.; Starikov, A. A.; Giovannetti, G.; Zwierzycki, M.; Talanana, M.; Brocks, G.; van den Brink, J.; Kelly, P. J. Theoretical Prediction of Perfect Spin Filtering at Interfaces between Close-Packed Surfaces of Ni or Co and Graphite or Graphene. *Phys. Rev. B* **2008**, *78*, 195419.

(9) Lakshmi, S.; Roche, S.; Cuniberti, G. Spin-Valve Effect in Zigzag Graphene Nanoribbons by Defect Engineering. *Phys. Rev. B* **2009**, *80*, 193404.

(10) Iqbal, M. Z.; Iqbal, M. W.; Lee, J. H.; Kim, Y. S.; Chun, S.-H.; Eom, J. Spin Valve Effect of NiFe/graphene/NiFe Junctions. *Nano Res.* **2013**, *6*, 373–380.

(11) Honda, S.; Yamamura, A.; Hiraiwa, T.; Sato, R.; Inoue, J.; Itoh, H. Magnetoresistance in Ferromagnetic-Metal/graphene/ferromagnetic-Metal Lateral Junctions. *Phys. Rev. B* **2010**, *82*, 033402.

(12) Geim, A. K.; Novoselov, K. S. The Rise of Graphene. *Nat. Mater.* **2007**, *6*, 183–191.

(13) Nagashima, A.; Tejima, N.; Oshima, C. Electronic States of the Pristine and Alkali-Metal-Intercalated Monolayer graphite/Ni(111) Systems. *Phys. Rev. B* **1994**, *50*, 17487–17495.

(14) Shikin, A. M.; Rybkin, A. G.; Marchenko, D.; Rybkina, A. A.; Scholz, M. R.; Rader, O.; Varykhalov, A. Induced Spin–orbit Splitting in Graphene: The Role of Atomic Number of the Intercalated Metal and Π–d Hybridization. *New J. Phys.* **2013**, *15*, 013016.

(15) Varykhalov, A.; Sánchez-Barriga, J.; Shikin, A. M.; Biswas, C.; Vescovo, E.; Rybkin, A.; Marchenko, D.; Rader, O. Electronic and Magnetic Properties of Quasifreestanding Graphene on Ni. *Phys. Rev. Lett.* **2008**, *101*, 157601.

(16) Hasegawa, M.; Nishidate, K.; Hosokai, T.; Yoshimoto, N. Electronic-Structure Modification of Graphene on Ni(111) Surface by the Intercalation of a Noble Metal. *Phys. Rev. B* **2013**, *87*, 085439.

(17) Varykhalov, A.; Sánchez-Barriga, J.; Shikin, A. M.; Biswas, C.; Vescovo, E.; Rybkin, A.; Marchenko, D.; Rader, O. Electronic and Magnetic Properties of Quasifreestanding Graphene on Ni. *Phys. Rev. Lett.* **2008**, *101*, 157601.

(18) Ligato, N.; Cupolillo, A.; Caputi, L. S. Study of the Intercalation of Graphene on Ni(111) with Cs Atoms: Towards the Quasi-Free Graphene. *Thin Solid Films* **2013**, *543*, 59–62.

(19) Wong, S. L.; Huang, H.; Wang, Y.; Cao, L.; Qi, D.; Santoso, I.; Chen, W.; Wee, A. T. S. Quasi-Free-Standing Epitaxial Graphene on SiC(0001) by Fluorine Intercalation from a Molecular Source. *ACS Nano* **2011**, *5*, 7662–7668.

(20) Grånäs, E.; Knudsen, J.; Schröder, U. A.; Gerber, T.; Busse, C.; Arman, M. A.; Schulte, K.; Andersen, J. N.; Michely, T. Oxygen Intercalation under Graphene on Ir(111): Energetics, Kinetics, and the Role of Graphene Edges. *ACS Nano* **2012**, *6*, 9951–9963.

(21) Zhao, W.; Kozlov, S. M.; Höfert, O.; Gotterbarm, K.; Lorenz, M. P. A.; Viñes, F.; Papp, C.; Görling, A.; Steinrück, H.-P. Graphene on Ni(111): Coexistence of Different Surface Structures. *J. Phys. Chem. Lett.* **2011**, *2*, 759–764.

(22) Bianchini, F.; Patera, L. L.; Peressi, M.; Africh, C.; Comelli, G. Atomic Scale Identification of Coexisting Graphene Structures on Ni(111). *J. Phys. Chem. Lett.* **2014**, *5*, 467–473.

(23) Dahal, A.; Batzill, M. Graphene–nickel Interfaces: A Review. *Nanoscale* **2014**, *6*, 2548–2562.

(24) Wintterlin, J.; Bocquet, M.-L. Graphene on Metal Surfaces. *Surf. Sci.* **2009**, *603*, 1841–1852.

(25) Wofford, J. M.; Starodub, E.; Walter, A. L.; Nie, S.; Bostwick, A.; Bartelt, N. C.; Thürmer, K.; Rotenberg, E.; McCarty, K. F.; Dubon, O. D. Extraordinary Epitaxial Alignment of Graphene Islands on Au(111). *New J. Phys.* **2012**, *14*, 053008.

(26) Voloshina, E. N.; Fertitta, E.; Garhofer, A.; Mittendorfer, F.; Fonin, M.; Thissen, A.; Dedkov, Y. S. Electronic Structure and Imaging Contrast of Graphene Moire on Metals. *Sci. Rep.* **2013**, *3*, 1072/1–7.

(27) Stojanov, P.; Voloshina, E.; Dedkov, Y.; Schmitt, S.; Haenke, T.; Thissen, A. Graphene on Rh(111): Combined DFT, STM, and NC-AFM Studies. *Procedia Eng.* **2014**, *93*, 8–16.

(28) Sutter, P. W.; Flege, J.-I.; Sutter, E. A. Epitaxial Graphene on Ruthenium. *Nat. Mater.* **2008**, *7*, 406–411.

(29) Nie, S.; Wu, W.; Xing, S.; Yu, Q.; Bao, J.; Pei, S.; McCarty, K. F. Growth from below: Bilayer Graphene on Copper by Chemical Vapor Deposition. *New J. Phys.* **2012**, *14*, 093028.

(30) Addou, R.; Dahal, A.; Sutter, P.; Batzill, M. Monolayer Graphene Growth on Ni(111) by Low Temperature Chemical Vapor Deposition. *Appl. Phys. Lett.* **2012**, *100*, 021601.

(31) Patera, L. L.; Africh, C.; Weatherup, R. S.; Blume, R.; Bhardwaj, S.; Castellarin-Cudia, C.; Knop-Gericke, A.; Schloegl, R.; Comelli, G.; Hofmann, S.; *et al.* In Situ Observations of the Atomistic Mechanisms of Ni Catalyzed Low Temperature Graphene Growth. *ACS Nano* **2013**, *7*, 7901–7912.

(32) Yu, Q.; Lian, J.; Siriponglert, S.; Li, H.; Chen, Y. P.; Pei, S.-S. Graphene Segregated on Ni Surfaces and Transferred to Insulators. *Appl. Phys. Lett.* **2008**, *93*, 113103.

(33) Zhang, Y.; Gao, T.; Xie, S.; Dai, B.; Fu, L.; Gao, Y.; Chen, Y.; Liu, M.; Liu, Z. Different Growth Behaviors of Ambient Pressure Chemical Vapor Deposition Graphene on Ni(111) and Ni Films: A Scanning Tunneling Microscopy Study. *Nano Res.* **2012**, *5*, 402–411.

(34) Lahiri, J.; Miller, T.; Adamska, L.; Oleynik, I. I.; Batzill, M. Graphene Growth on Ni(111) by Transformation of a Surface Carbide. *Nano Lett.* **2011**, *11*, 518–522.

(35) Jacobson, P.; Stöger, B.; Garhofer, A.; Parkinson, G. S.; Schmid, M.; Caudillo, R.; Mittendorfer, F.; Redinger, J.; Diebold, U. Nickel Carbide as a Source of Grain Rotation in Epitaxial Graphene. *ACS Nano* **2012**, *6*, 3564–3572.

(36) Song, J. Structural, Electronic and Magnetic Properties of Ultrathin Epitaxial Manganese Films, Freie Universität Berlin, Germany, **2015**, http://www.diss.fu-berlin.de/diss/receive/FUDISS_thesis_000000100345.

(37) Weatherup, R. S.; Amara, H.; Blume, R.; Dlubak, B.; Bayer, B. C.; Diarra, M.; Bahri, M.; Cabrero-Vilatela, A.; Caneva, S.; Kidambi, P. R.; *et al.* Interdependency of Subsurface Carbon Distribution and Graphene–Catalyst Interaction. *J. Am. Chem. Soc.* **2014**, *136*, 13698–13708.

(38) Zhao, R.; Zhang, Y.; Gao, T.; Gao, Y.; Liu, N.; Fu, L.; Liu, Z. Scanning Tunneling Microscope Observations of Non-AB Stacking of Graphene on Ni Films. *Nano Res.* **2011**, *4*, 712–721.

(39) Zhang, Y.; Gao, T.; Xie, S.; Dai, B.; Fu, L.; Gao, Y.; Chen, Y.; Liu, M.; Liu, Z. Different Growth Behaviors of Ambient Pressure Chemical Vapor Deposition Graphene on Ni(111) and Ni Films: A Scanning Tunneling Microscopy Study. *Nano Res.* **2012**, *5*, 402–411.

(40) Olsen, T.; Yan, J.; Mortensen, J. J.; Thygesen, K. S. Dispersive and Covalent Interactions between Graphene and Metal Surfaces from the Random Phase Approximation. *Phys. Rev. Lett.* **2011**, *107*, 156401.

(41) Dahal, A.; Addou, R.; Sutter, P.; Batzill, M. Graphene Monolayer Rotation on Ni(111) Facilitates Bilayer Graphene Growth. *Appl. Phys. Lett.* **2012**, *100*, 241602.

(42) Pong, W.-T.; Durkan, C. A Review and Outlook for an Anomaly of Scanning Tunnelling Microscopy (STM): Superlattices on Graphite. *J. Phys. Appl. Phys.* **2005**, *38*, R329.

(43) Osing, J.; Shvets, I. V. Bulk Defects in Graphite Observed with a Scanning Tunnelling Microscope. *Surf. Sci.* **1998**, *417*, 145–150.

(44) Garbarz, J.; Lacaze, E.; Faivre, G.; Gauthier, S.; Schott, M. Dislocation Networks in Graphite: A Scanning Tunnelling Microscopy Study. *Philos. Mag. A* **1992**, *65*, 853–861.

(45) Albrecht, T. R.; Mizes, H. A.; Nogami, J.; Park, S.; Quate, C. F. Observation of Tilt Boundaries in Graphite by Scanning Tunneling Microscopy and Associated Multiple Tip Effects. *Appl. Phys. Lett.* **1988**, *52*, 362–364.

(46) Kuwabara, M.; Clarke, D. R.; Smith, D. A. Anomalous Superperiodicity in Scanning Tunneling Microscope Images of Graphite. *Appl. Phys. Lett.* **1990**, *56*, 2396–2398.

(47) Buckley, J. E.; Wragg, J. L.; White, H. W.; Bruckdorfer, A.; Worcester, D. L. Large-scale Periodic Features Associated with Surface Boundaries in Scanning Tunneling Microscope Images of Graphite. *J. Vac. Sci. Technol. B* **1991**, *9*, 1079–1082.

(48) Kuwabara, M.; Clarke, D. R.; Smith, D. A. Anomalous Superperiodicity in Scanning Tunneling Microscope Images of Graphite. *Appl. Phys. Lett.* **1990**, *56*, 2396–2398.

(49) Liu, C. Y.; Chang, H.; Bard, A. J. Large Scale Hexagonal Domainlike Structures Superimposed on the Atomic Corrugation of a Graphite Surface Observed by Scanning Tunneling Microscopy. *Langmuir* **1991**, *7*, 1138–1142.

(50) Green, T.; Weigle, J. Theorie Du Moire. *Helvetica Phys. Acta* **1948**, *21*, 217–217.

(51) Oster, G. Moire Patterns in Physics. *Endeavour* **1968**, *27*, 60–64.

(52) Murata, Y.; Petrova, V.; Kappes, B. B.; Ebnonnasir, A.; Petrov, I.; Xie, Y.-H.; Ciobanu, C. V.; Kodambaka, S. Moiré Superstructures of Graphene on Faceted Nickel Islands. *ACS Nano* **2010**, *4*, 6509–6514.

(53) Rong, Z. Y.; Kuiper, P. Electronic Effects in Scanning Tunneling Microscopy: Moiré Pattern on a Graphite Surface. *Phys. Rev. B* **1993**, *48*, 17427–17431.

(54) Bernhardt, T. M.; Kaiser, B.; Rademann, K. Formation of Superperiodic Patterns on Highly Oriented Pyrolytic Graphite by Manipulation of Nanosized Graphite Sheets with the STM Tip. *Surf. Sci.* **1998**, *408*, 86–94.

(55) Xhie, J.; Sattler, K.; Ge, M.; Venkateswaran, N. Giant and Supergiant Lattices on Graphite. *Phys. Rev. B* **1993**, *47*, 15835–15841.

(56) Biró, L. P.; Lambin, P. Grain Boundaries in Graphene Grown by Chemical Vapor Deposition. *New J. Phys.* **2013**, *15*, 035024.

(57) Sun, H.-L.; Shen, Q.-T.; Jia, J.-F.; Zhang, Q.-Z.; Xue, Q.-K. Scanning Tunneling Microscopy Study of Superlattice Domain Boundaries on Graphite Surface. *Surf. Sci.* **2003**, *542*, 94–100.

(58) Oden, P. I.; Thundat, T.; Nagahara, L. A.; Lindsay, S. M.; Adams, G. B.; Sankey, O. F. Superperiodic Features Observed on Graphite under Solution with Scanning Tunneling Microscopy. *Surf. Sci.* **1991**, *254*, L454–L459.

(59) Batzill, M. The Surface Science of Graphene: Metal Interfaces, CVD Synthesis, Nanoribbons, Chemical Modifications, and Defects. *Surf. Sci. Rep.* **2012**, *67*, 83–115.

(60) Morell, E. S.; Vargas, P.; Häberle, P.; Hevia, S. A.; Chico, L. Edge States of Moiré Structures in Graphite. *Phys. Rev. B* **2015**, *91*, 035441.

(61) Biró, L. P.; Lambin, P. Grain Boundaries in Graphene Grown by Chemical Vapor Deposition. *New J. Phys.* **2013**, *15*, 035024.

(62) Červenka, J.; Flipse, C. F. J. Structural and Electronic Properties of Grain Boundaries in Graphite: Planes of Periodically Distributed Point Defects. *Phys. Rev. B* **2009**, *79*, 195429.

(63) Warner, J. H.; Rümmeli, M. H.; Gemming, T.; Büchner, B.; Briggs, G. A. D. Direct Imaging of Rotational Stacking Faults in Few Layer Graphene. *Nano Lett.* **2009**, *9*, 102–106.

(64) Vázquez de Parga, A. L.; Calleja, F.; Borca, B.; Passeggi, M. C. G.; Hinarejos, J. J.; Guinea, F.; Miranda, R. Periodically Rippled Graphene: Growth and Spatially Resolved Electronic Structure. *Phys. Rev. Lett.* **2008**, *100*, 056807.

(65) Borca, B.; Barja, S.; Garnica, M.; Hinarejos, J. J.; Vázquez de Parga, A. L.; Miranda, R.; Guinea, F. Periodically Modulated Geometric and Electronic Structure of Graphene on Ru(0001). *Semicond. Sci. Technol.* **2010**, *25*, 034001.

(66) Jiang, D.; Du, M.-H.; Dai, S. First Principles Study of the graphene/Ru(0001) Interface. *J. Chem. Phys.* **2009**, *130*, 074705.

(67) Wang, B.; Bocquet, M.-L.; Marchini, S.; Günther, S.; Wintterlin, J. Chemical Origin of a Graphene Moiré Overlayer on Ru(0001). *Phys. Chem. Chem. Phys.* **2008**, *10*, 3530–3534.

(68) Feng, W.; Lei, S.; Li, Q.; Zhao, A. Periodically Modulated Electronic Properties of the Epitaxial Monolayer Graphene on Ru(0001). *J. Phys. Chem. C* **2011**, *115*, 24858–24864.

(69) Varykhalov, A.; Marchenko, D.; Sánchez-Barriga, J.; Scholz, M. R.; Verberck, B.; Trauzettel, B.; Wehling, T. O.; Carbone, C.; Rader, O. Intact Dirac Cones at Broken Sublattice Symmetry: Photoemission Study of Graphene on Ni and Co. *Phys. Rev. X* **2012**, *2*, 041017.

(70) Grüneis, A.; Vyalikh, D. V. Tunable Hybridization between Electronic States of Graphene and a Metal Surface. *Phys. Rev. B* **2008**, *77*, 193401.

(71) Generalov, A. V.; Voloshina, E. N.; Dedkov, Y. S. Structural and Electronic Properties of Graphene-Based Junctions for Spin-Filtering: The graphene/Al/Ni(111) Intercalation-like System. *Appl. Surf. Sci.* **2013**, *267*, 8–11.

(72) Sánchez-Barriga, J.; Varykhalov, A.; Scholz, M. R.; Rader, O.; Marchenko, D.; Rybkin, A.; Shikin, A. M.; Vescovo, E. Chemical Vapour Deposition of Graphene on Ni(111) and Co(0001) and Intercalation with Au to Study Dirac-Cone Formation and Rashba Splitting. *Diam. Relat. Mater.* **2010**, *19*, 734–741.

(73) Kang, M. H.; Jung, S. C.; Park, J. W. Density Functional Study of the Au-Intercalated graphene/Ni(111) Surface. *Phys. Rev. B* **2010**, *82*, 085409.

(74) Generalov, A. V.; Dedkov, Y. S. EELS Study of the Epitaxial graphene/Ni(111) and graphene/Au/Ni(111) Systems. *Carbon* **2012**, *50*, 183–191.

(75) Bertoni, G.; Calmels, L.; Altibelli, A.; Serin, V. First-Principles Calculation of the Electronic Structure and EELS Spectra at the graphene/Ni(111) Interface. *Phys. Rev. B* **2005**, *71*, 075402.

(76) Shikin, A. M.; Prudnikova, G. V.; Adamchuk, V. K.; Moresco, F.; Rieder, K.-H. Surface Intercalation of Gold underneath a Graphite Monolayer on Ni(111) Studied by Angle-Resolved Photoemission and High-Resolution Electron-Energy-Loss Spectroscopy. *Phys. Rev. B* **2000**, *62*, 13202–13208.

(77) Grüneis, A. Synthesis and Electronic Properties of Chemically Functionalized Graphene on Metal Surfaces. *J. Phys. Condens. Matter* **2013**, *25*, 043001.

(78) Kwon, S. G.; Kang, M. H. Effects of Cu Intercalation on the graphene/Ni(111) Surface: Density-Functional Calculations. *J. Korean Phys. Soc.* **2012**, *61*, 589–593.

(79) Sun, X.; Pratt, A.; Yamauchi, Y. First-Principles Study of the Structural and Magnetic Properties of Graphene on a Fe/Ni(111) Surface. *J. Phys. Appl. Phys.* **2010**, *43*, 385002.

(80) Kelty, S. P.; Lieber, C. M. Scanning Tunneling Microscopy Investigations of the Electronic Structure of Potassium-Graphite Intercalation Compounds. *J. Phys. Chem.* **1989**, *93*, 5983–5985.

(81) Grüneis, A.; Vyalikh, D. V. Tunable Hybridization between Electronic States of Graphene and a Metal Surface. *Phys. Rev. B* **2008**, *77*, 193401.

(82) Park, Y. S.; Park, J. H.; Hwang, H. N.; Laishram, T. S.; Kim, K. S.; Kang, M. H.; Hwang, C. C. Quasi-Free-Standing Graphene Monolayer on a Ni Crystal through Spontaneous Na Intercalation. *Phys. Rev. X* **2014**, *4*, 031016.

(83) Adamska, L.; Addou, R.; Batzill, M.; Oleynik, I. I. Atomic and Electronic Structure of graphene/Sn-Ni(111) and graphene/Sn-Cu(111) Surface Alloy Interfaces. *Appl. Phys. Lett.* **2012**, *101*, 051602.

(84) Addou, R.; Dahal, A.; Batzill, M. Graphene on Ordered Ni-Alloy Surfaces Formed by Metal (Sn, Al) Intercalation between graphene/Ni(111). *Surf. Sci.* **2012**, *606*, 1108–1112.

(85) Vita, H.; Böttcher, S.; Leicht, P.; Horn, K.; Shick, A. B.; Máca, F. Electronic Structure and Magnetic Properties of Cobalt Intercalated in Graphene on Ir(111). *Phys. Rev. B* **2014**, *90*, 165432.

(86) Weser, M.; Voloshina, E. N.; Horn, K.; Dedkov, Y. S. Electronic Structure and Magnetic Properties of the graphene/Fe/Ni(111) Intercalation-like System. *Phys. Chem. Chem. Phys.* **2011**, *13*, 7534–7539.

(87) Zhang, W.-B.; Chen, C. Tuning Metal–graphene Interaction by Non-Metal Intercalation: A Case Study of the graphene/oxygen/Ni(111) System. *J. Phys. Appl. Phys.* **2015**, *48*, 015308.

(88) Grüneis, A. Synthesis and Electronic Properties of Chemically Functionalized Graphene on Metal Surfaces. *J. Phys. Condens. Matter* **2013**, *25*, 043001.

(89) Riedl, C.; Coletti, C.; Iwasaki, T.; Zakharov, A. A.; Starke, U. Quasi-Free-Standing Epitaxial Graphene on SiC Obtained by Hydrogen Intercalation. *Phys. Rev. Lett.* **2009**, *103*, 246804.

(90) Larciprete, R.; Ulstrup, S.; Lacovig, P.; Dalmiglio, M.; Bianchi, M.; Mazzola, F.; Hornekær, L.; Orlando, F.; Baraldi, A.; Hofmann, P.; *et al*. Oxygen Switching of the Epitaxial Graphene–Metal Interaction. *ACS Nano* **2012**, *6*, 9551–9558.

(91) Dedkov, Y. S.; Fonin, M.; Laubschat, C. A Possible Source of Spin-Polarized Electrons: The Inert graphene/Ni(111) System. *Appl. Phys. Lett.* **2008**, *92*, 052506.

(92) Weatherup, R. S.; D'Arsié, L.; Cabrero-Vilatela, A.; Caneva, S.; Blume, R.; Robertson, J.; Schloegl, R.; Hofmann, S. Long-Term Passivation of Strongly Interacting Metals with Single-Layer Graphene. *J. Am. Chem. Soc.* **2015**, *137*, 14358–14366.

(93) Sutter, P.; Sadowski, J. T.; Sutter, E. A. Chemistry under Cover: Tuning Metal–Graphene Interaction by Reactive Intercalation. *J. Am. Chem. Soc.* **2010**, *132*, 8175–8179.

(94) Zhang, H.; Fu, Q.; Cui, Y.; Tan, D.; Bao, X. Growth Mechanism of Graphene on Ru(0001) and O2 Adsorption on the Graphene/Ru(0001) Surface. *J. Phys. Chem. C* **2009**, *113*, 8296–8301.

(95) Mehmood, F.; Pachter, R.; Lu, W.; Boeckl, J. J. Adsorption and Diffusion of Oxygen on Single-Layer Graphene with Topological Defects. *J. Phys. Chem. C* **2013**, *117*, 10366–10374.

Table of Contents Image: